Tellus (1990), *42A*, 568–582

A coupled one-dimensional sea ice–ocean model applied to a semi-enclosed basin

By ANDERS OMSTEDT, *SMHI, S-601 76 Norrköping, Sweden*

(Manuscript received 14 April 1989; in final form 17 November 1989)

ABSTRACT

The objectives of the present study are to formulate and explore a coupled sea ice–ocean model for semi-enclosed basins. Both thermodynamic and dynamic processes are included. Variations in the on–off shore directions are considered, and the model is applied to the Bothnian Bay, where ridging due to southerly winds is a common feature. The importance of the different ice processes and their simulation are discussed. It is concluded that a one-dimensional model approach to the winter sea ice season can be used, giving realistic information about ice formation, growth and decay. Horizontal gradients in the sea and in the ice, however, imply that a two- or three-dimensional model is in general needed, particularly for the initial advance of the ice edge and for the ice deformation calculation.

1. Introduction

The modelling of the thermal regime in different sub-basins in the Baltic Sea has been subject to several investigations (Omstedt, 1990). In that study, the whole winter period was analysed, using a model, which divided the Baltic Sea into thirteen sub-basins, together with data from the severe winter of 1986/87. Sea ice was, however, not dealt with in the model; instead boundary conditions for an open water surface were applied all through the season, and the water temperatures were put equal to the freezing point when they were below freezing. Reasonable results were achieved, but it was concluded that sea ice had to be considered in some of the thirteen sub-basins. For example, the calculations indicated that sea ice could delay spring warming for more than one month in the Bothnian Bay (Fig. 1). The purpose of the present work is therefore to formulate and explore a mathematical model of sea ice, which could be incorporated into one-dimensional ocean models. Only variations in the on–off shore directions will be considered, and the model will be applied to the Bothnian Bay, where ridging due to southerly wind is a common feature.

The formation, growth and decay of a sea ice cover is in an intricate balance of both thermal and dynamic variations. The ice cover is also influenced by the presence of coastal processes such as, for example, compression during on-shore ice drift and formation of polynyas during off-shore ice drift. The sea ice interacts with the ocean, partly due to thermal effects and partly to buoyancy effects associated with the ice/water salinity exchange during freezing and melting. The exchange of momentum between the atmosphere and the ocean is also influenced by sea ice. Some basic studies of interest to the present work will be reviewed.

Sea ice dynamics have been the subject of many studies, see, e.g., Hibler (1986). The general approach is to consider the ice to be a two-dimensional continuum and to introduce a constitutive law, which simulates the behaviour of ridged ice. The basic state variables are the ice thickness and the ice concentration, and effects due to different ice types, ice temperatures, etc., are generally not taken into consideration. The ice drift is determined from a momentum balance, which considers the acceleration, the Coriolis force, the ocean surface tilt, the air and water stress, and the internal force due to ice

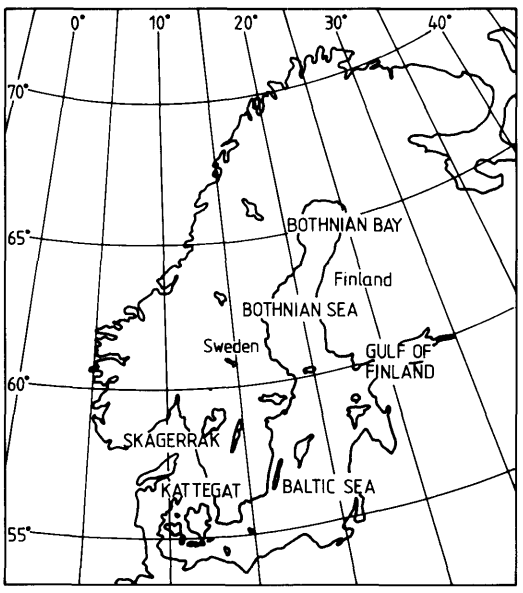

Fig. 1. Map of the water surrounding Scandinavia.

interaction. The ice strength takes into account the fact that thin ice resists compression less than thick ice. In coastal regions a somewhat different constitutive law has been proposed by Overland and Pease (1988). In general the sea ice strength has to be considered only during converging drift at high ice concentrations. At diverging ice drift, the strength is reduced due to the presence of cracks and leads. The dynamic coupling of sea ice and underlying current is another basic problem in sea ice dynamics; see, e.g., McPhee (1986). This problem is further discussed by Leppäranta and Omstedt (1990) in an investigation of sea ice drift and currents in the Bothnian Bay.

Modelling thermal variations in an ice–ocean system, one has to consider both vertical and horizontal variations. Thermodynamic sea ice models, which often only consider vertical variations, use the heat equation for ice and snow and introduce different heat flux formulations for the interaction with the atmosphere, see Maykut (1986) or Leppäranta (1983) and Stössel (1985) for applications in the Baltic Sea. Some recent thermodynamic models also include leads, e.g., Fichefet and Gasper (1988). In these models, the main unknown heat flux is the heat from the ocean to the ice, which implies a need for coupled ice–ocean models, see, e.g., Røed (1984) or Lemke (1987). This is particularly true in the case of the marginal ice zone and during freezing and melting. In these cases advective effects as well as surface water mixing can cause heat flows to the ice of considerable values. When modelling sea ice during melting and freezing, the viscous sublayers at the ice/water interface also have to be introduced; see further discussion in McPhee et al. (1987) or Svensson and Omstedt (1990). Modelling ice formation in turbulent waters, one has also to consider ice in suspension (Frazil Ice); see Bauer and Martin (1983) or Omstedt (1985). A model for Frazil Ice formation in wind-driven polynyas was presented by Pease (1987). In that model, the polynya width was examined by considering a balance between ice drift and ice formation. Similar ideas will also be applied to the present model. In the case of horizontal decay, ice ridging as well as melting can decrease the ice cover. For the melting of a sea ice cover, the short-wave radiation entering the water and the ice had to be considered, see Langleben (1972) and Maykut and Perovitch (1987). The importance of sun radiation through the ice during spring warming is further discussed by Sahlberg (1988), where a one-dimensional lake model, with thermal effects due to ice and snow, is presented.

In Section 2, the mathematical formulation is outlined. In Section 3, some details of calculations are given. In Section 4, the model is tested during idealized conditions. Verification studies from three winter seasons are presented in Section 5. Section 6 discusses the model and its applicability. Finally, in Section 7, a summary is given and some conclusions are drawn.

2. Model

2.1. Basic assumptions

The study will restrict its attention to variations in the direction perpendicular to a shore (Fig. 2). It will be assumed that the ice moves freely in the case of off-shore winds and deforms as a plastic material, in the case of on-shore winds. The horizontal growth and decay due to thermal processes are assumed to be due to a formation/melting speed, which is an effect of the net heat energy budget over the open water

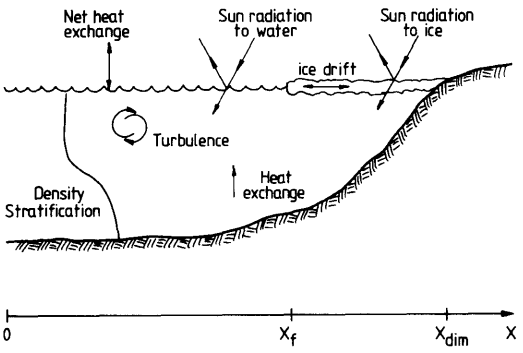

Fig. 2. A sketch of the problem under consideration.

area. In the case of ice formation, a constant new ice thickness of 0.1 m is assumed. In the case of melting, the horizontal mean ice thickness over the whole ice cover is assumed to be more relevant.

In the energy budget, fluxes due to sensible heat, latent heat, net long-wave radiation, short-wave radiation and heat from the ocean are included. Short-wave radiation through the ice into the water is also considered. The heat fluxes are calculated from bulk formulas and the heat flux from the ocean is determined from a one-dimensional ocean model.

In the ocean model, only vertical variations are considered. This implies that the ocean is assumed to be horizontally homogeneous under the ice cover. Thus neither horizontal temperature gradients in the ocean nor advective effects are taken into consideration. The turbulent mixing is assumed to be caused by current shear and salt rejection from the freezing ice. Wall functions for a rough surface are introduced at the ice/water interface to simulate molecular effects. Ridging and rafting are assumed to change the mean ice thickness, but a constant roughness parameter at the ice/water interface is assumed all through the winter season.

2.2. *Ice drift*

Deformation due to on-shore winds and spreading due to off-shore winds are of main interest. The model for plastic ice deformation in the Marginal Ice Zone by Leppäranta and Hibler (1985) is used as a starting point. If only variations in the on-shore x-direction are considered (neglecting the acceleration, the Coriolis force and the ocean surface tilt), the ice drift equation reads:

$$\frac{d\sigma}{dx} + \tau_{wx} + \tau_{ax} = 0, \tag{1}$$

where σ is the ice stress tensor, τ_{wx} and τ_{ax} the water and the air stress respectively. If one further assumes pure plastic drift, the ice stress tensor is reduced to:

$$\sigma = \begin{cases} -P & \text{when } \dfrac{du_i}{dx} < 0, \\ 0 & \text{when } \dfrac{du_i}{dx} \geqslant 0, \end{cases} \tag{2}$$

where P is the ice strength.

The parameterization of the ice strength follows that by Overland and Pease (1988), where

$$P = \rho_i \mu_0 h_i^2 \exp(-C(1 - A_i)). \tag{3}$$

In eq. (3), h_i is the ice thickness, ρ_i the ice density, A_i the ice concentration, μ_0 and C constants. The ice strength formulation is further discussed in Subsection 4.1.

The ice drift equation becomes:

$$\begin{cases} \tau_{wx} + \tau_{ax} - \dfrac{dP}{dx} = 0, & \text{when } \dfrac{du_i}{dx} < 0; \quad \text{(a)} \\ \tau_{wx} + \tau_{ax} = 0, & \text{when } \dfrac{du_i}{dx} \geqslant 0. \quad \text{(b)} \end{cases} \tag{4}$$

The solution of eq. (4b) is the free drift ice velocity (u_{free}). If linear water stress laws are assumed and eq. (4a) is integrated from the ice front ($x = X_f$) to the shore ($x = X_{dim}$), the solution becomes:

$$\begin{cases} u_i = u_{free} - \dfrac{P(X_{dim})}{k(X_{dim} - X_f)} & \tau_a > 0, \\ u_i = u_{free} & \tau_a \leqslant 0, \end{cases} \tag{5}$$

where $(X_{dim} - X_f)$ is the ice cover extension and, when divided with the characteristic length of the basin, equal to the ice concentration ($A_i = (X_{dim} - X_f)/X_{dim}$). The linear friction coefficient in the water stress formulation is denoted by k. The position of the ice front, X_f, is defined as the length of the open water outside the ice pack (see Fig. 2). It becomes zero when the sea is fully ice-covered, and X_{dim} when no ice is present.

The plastic behaviour of the ice drift is thus due to the ice strength, which can reduce the free ice drift down to zero during converging motion.

2.3. *Heat fluxes and ice cover*

The change of the horizontal extent of the ice is assumed to be due to the ice drift and the ice formation/melting rate. The equation reads:

$$\frac{dX_f}{dt} = u_i - \frac{X_f}{h_{eff}} \frac{Q_{nw}}{\rho_i L_i}, \tag{6}$$

where Q_{nw} is the net heat balance at the open water surface, h_{eff} the effective ice thickness defined as the horizontal mean ice thickness in the freezing/melting region, and L_i the latent heat of ice. The equation implies that all net heat energy at the open water surface goes to lateral freezing or melting. Freezing or warming of the water outside the ice pack is thus not dealt with. During ice formation, the ice types are either Frazil Ice or Nilas. The effective ice thickness is assumed to be the same in both cases with a typical thickness of 0.1 m. In the case of melting ice, the horizontal mean ice thickness over the whole ice cover is assumed to be a more appropriate thickness.

The ice thickness is partly due to ridging and partly due to vertical growth or melting. The equation for vertical growth/melting reads:

$$\rho_i L \frac{dh_i}{dt} = \frac{k_i k_s}{k_i h_s + k_s h_i} (T_f - T_0) + Q_w, \tag{7}$$

where h_i and h_s is the ice and snow thickness, k_i and k_s the thermal conductivity of ice and snow, T_f the water freezing temperature, T_0 the temperature at the air/snow interface, and Q_w the heat flux from the sea to the ice. The air/snow interface temperature can be obtained by considering the heat energy budget over the snow cover, see Maykut (1986). This is, however, not done in the present paper. Instead T_0 is assumed to be equal to the air temperature as long as the temperature is below freezing. For air temperature above freezing, only melting due to ocean heat is calculated, and surface melting is thus not dealt with.

The net heat balance in eq. (6) is an outcome of the heat budget over the open water surface. In this budget several different fluxes have to be considered. The net heat flux to the air/water interface reads:

$$Q_{nw} = Q_h + Q_e + Q_{\ell u} - Q_{\ell d} + Q_w, \tag{8}$$

where Q_h is the sensible heat flux, Q_e the latent heat flux, $Q_{\ell u}$ the long-wave radiation upwards, $Q_{\ell d}$ the long-wave radiation downwards, and Q_w the heat flux from the sea.

The sensible and latent heat fluxes are caused by the temperature and the moisture differences between water/air respectively. The parameterization follows Friehe and Schmitt (1976), where different transfer coefficients are introduced depending on stratification conditions. The fluxes read:

$$Q_h = \rho_a c_{pa} (C_1 + C_h U_a (T_s - T_a)), \tag{9}$$

$$Q_e = L_e C_e U_a (q_w - q_a), \tag{10}$$

where ρ_a ($= 1.3$ kg m^{-3}) is the air density, c_{pa} ($= 1016$ J kg^{-1} K^{-1}) the specific heat of air, C_h and C_e the sensible heat and the latent heat transfer coefficients respectively, C_1 a constant, T_s the surface water temperature, U_a the wind velocity at 10 m, L_e ($= 2.5 \cdot 10^6$ J kg^{-1}) the latent heat of evaporation, q_w and q_a the water vapour density close to the water surface and in the atmosphere respectively. The numbers put in brackets are values used in the present application. Measurements of q_w and q_a are not directly available, instead they are transformed to functions of temperatures and relative humidity. The heat transfer coefficients read:

$$(C_1, C_h) = \begin{cases} 0.0026,\ 0.86 \cdot 10^{-3} & \text{when } U_s(T_s - T_a) < 0, \\ 0.002,\ 0.97 \cdot 10^{-3} & \text{when } O \leqslant U_s(T_s - T_a) \leqslant 25, \\ 0.0,\ 1.46 \cdot 10^{-3} & \text{when } U_s(T_s - T_a) > 25, \end{cases}$$

and $C_e = 1.36 C_h$ for all stabilities.

The net long-wave radiation is due to atmospherical and water surface radiation. The formulation reads:

$$Q_{\ell u} - Q_{\ell d} = \varepsilon_w \sigma_s [T_w^4 - T_a^4 (a_1 + a_2 \sqrt{e_a})(1 + a_3 N_a^2)], \tag{11}$$

where ε_w ($= 0.97$) is the emissivity of the water surface, e_a the water vapour pressure in the atmosphere, σ_s ($= 5.67 \cdot 10^{-8}$ W m^{-2} K^{-4}) the Stefan Bolzman's constant, N_a the cloud coverage, and a_1, a_2 and a_3 are constants equal to 0.68, 0.0036 and 0.18, respectively.

Short-wave radiation penetrates down into the water column either through the open sea surface or through the ice cover, and increases the heat content due to internal absorption. The short wave energy flux penetrating the open water surface reads:

$$Q_s^w = Q_s(1 - \alpha_w), \tag{12}$$

where Q_s is the insolation towards the surface and α_w is the surface water albedo calculated from the Fresnels formula.

The insolation towards the ground can be calculated from:

$$Q_s = T_u S_0 \cos\Theta(T_r - A_w)(1 - N_a F_a), \tag{13}$$

where T_u is the atmospherical turbidity which is put equal to 0.95, S_0 ($= 1.36 \cdot 10^3$ J m^{-2} s^{-1}) the solar constant, Θ the zenith angle, T_r and A_w are transmission and absorption functions, and F_a is a cloud function. The short and long wave formulations follow those by Bodin (1979), but with only the total cloud amount considered in the present application. The expressions then read:

$$F_a = 0.55 + 0.01 \cos\Theta^{-1},$$

$$T_r = 1.041 - 0.16 \cos\Theta^{-0.5},$$

$$A_w = 0.077 m^{0.3} \cos\Theta^{-0.3},$$

where m is the optical path length, which is calculated as a function of season.

The modelling of the short-wave radiation, which penetrates snow and ice, follows that by Sahlberg (1988). The equation reads:

$$Q_s^i = Q_s(1 - \alpha_s)\, i_{os}\, e^{-\bar{K}_s(h_s - 0.1) - \bar{K}_i h_i} \tag{14}$$

where α_s ($= 0.75$) is the snow albedo, i_{os} ($= 0.1$) is a penetration factor, h_s the snow thickness, h_i the ice thickness, $\bar{K}_s$ ($= 15$ m^{-1}) and $\bar{K}_i$ ($= 1.5$ m^{-1}) the bulk extinction coefficients for snow and ice, respectively. Basic assumptions in eq. (14) are that slush is not present and that the snow depth is equal or larger than 0.1 m.

The solar radiation penetrates down into the water column and increases the heat content due to internal absorption. An exponential decay law is assumed, and the heat source term S_h due to solar radiation to the open water surface and through the ice reads:

$$S_h = [Q_s^w(1 - \eta)(1 - A_i) + Q_s^i A_i]\beta e^{-\beta(D - z)}, \tag{15}$$

where η is a measurement of the infrared content of the solar radiation, D the total water depth, z the vertical space coordinate positive upwards, and β an absorption coefficient. The constants η and β are put equal to 0.4 and 0.3, respectively.

The final heat flow to be considered is the heat from deeper layers (Q_w). In most heat budgets this is the unknown part, and in general only constant values are used. In the present model we calculate this flux from the ocean model presented below. The heat flux formulation then reads:

$$Q_w = \frac{\nu_T}{\sigma_H} \frac{\partial}{\partial z}(\rho C_p T), \tag{16}$$

where ρ is the density of water, C_p the specific heat of water, T the water temperature, ν_T the eddy viscosity and σ_H the turbulent Prandtl number. The heat flux is assumed to decrease partly the ice thickness (A_i) and partly the horizontal ice cover growth ($1 - A_i$).

2.4. *Mean ocean equations*

Primarily it is the heat fluxes from the ocean to the atmosphere or the ice that are of main interest, but some more variables are needed to describe the upper layers of the ocean. Salinity is one of these, as well as velocity. For basic assumptions etc., see Omstedt et al. (1983).

$$\frac{\partial}{\partial t}(\rho C_p T) = \left[\frac{\partial}{\partial z}\frac{\nu_T}{\sigma_H}\frac{\partial}{\partial z}(\rho C_p T)\right] + S_h, \tag{17}$$

$$\frac{\partial S}{\partial t} = \frac{\partial}{\partial z}\left(\frac{\nu_T}{\sigma_S}\frac{\partial S}{\partial z}\right), \tag{18}$$

$$\frac{\partial \rho U}{\partial t} = \frac{\partial}{\partial z}\left(\nu_T \frac{\partial \rho U}{\partial z}\right) + f\rho V, \tag{19}$$

$$\frac{\partial \rho V}{\partial t} = \frac{\partial}{\partial z}\left(\nu_T \frac{\partial \rho V}{\partial z}\right) - f\rho U, \tag{20}$$

$$\rho = \rho_0[1 - \alpha_1(T - T_M)^2 + \alpha_2 S], \tag{21}$$

where z is the vertical space coordinate positive upwards, t is the time coordinate, S the salinity, σ_S the turbulent Schmidt number, U and V are the mean currents in horizontal directions, f is the Coriolis' parameter, ρ_0 a reference density, T_M the temperature of maximum density, and α_1 and α_2 are constants in the equation of state.

The boundary conditions for an open water surface read:

$$\frac{\nu_T}{\sigma_H}\frac{\partial T}{\partial z} = Q_{nw}(\rho_0 C_p)^{-1}, \tag{22}$$

$$\frac{\nu_T}{\sigma_S}\frac{\partial S}{\partial z}=0, \tag{23}$$

$$\nu_T\frac{\partial U}{\partial z}=-\tau_{xa}\rho_0^{-1}, \tag{24}$$

$$\nu_T\frac{\partial V}{\partial z}=-\tau_{ya}\rho_0^{-1}, \tag{25}$$

where τ_{xa} and τ_{ya} are the wind stresses in the x- and y-directions. A zero flux condition is assumed for the salinity equation, even though precipitation and evaporation may produce a net heat flux.

In the case of ice, the most obvious boundary condition for temperature is the fact that the interfacial temperature is equal to the freezing/melting temperature:

$$T=T_f=-m_1 S_0, \tag{26}$$

where S_0 is the interfacial salinity and m_1 a constant equal to 0.06. The boundary condition for salinity at the ice/water interface is assumed to be related to the freezing and melting rate:

$$\frac{\nu_T}{\sigma_s}\frac{\partial S}{\partial z}=(S_i-S_0)\frac{\partial h_i'}{\partial t}, \tag{27}$$

where S_i is the ice salinity and h_i' is defined as the horizontal mean ice thickness due to thermodynamic forcing. Thus ridging is not included in h_i'. The corresponding boundary conditions for momentum is that the current velocities are equal to the ice drift at the ice/water interface. The conditions for the lower boundary are no flux conditions, except for velocity, for which a zero velocity condition is used.

In the boundary conditions given in eqs. (26) and (27), the interfacial salinity (S_0), and the freezing temperature (T_f) have to be calculated. They do not, however, have any obvious value; instead they are an outcome of the balance between the melting or freezing rate and the turbulent mixing outside the viscous sublayer.

To bridge the fully turbulent ocean layer beneath the drifting ice and the viscous sublayer adjacent to the ice, two model approaches are available today. The first one introduces wall functions, Mellor et al. (1986) and puts the near-wall mesh point into the fully turbulent fluid. The second one introduces a low-Reynolds' number turbulence model for the viscous region, Svensson and Omstedt (1990), and resolves the whole boundary layer all the way into the ice.

McPhee et al. (1987) tested different wall function formulations and illustrated that fully turbulent models predicted unrealistically high melting rates and that the viscous sublayer models underestimated melting. Quite realistic values were, however, received using a wall function formulation according to Yaglom and Kader (1974). In the present paper we shall follow that path, and the wall functions read:

$$\mathrm{St}_T^{-1}=b\left(\frac{u_* z_0}{\nu}\right)^{0.5}\mathrm{Pr}_L^{0.67}, \tag{28}$$

$$\mathrm{St}_S^{-1}=b\left(\frac{u_* z_0}{\nu}\right)^{0.5}\mathrm{Sc}_L^{0.67}, \tag{29}$$

where St_T and St_S are the Stanton numbers for temperature and salinity respectively, b (= 1.57) is a constant, u_* the friction velocity, z_0 the roughness parameter, Pr_L (= 13.8) the laminar Prandtl number and Sc_L (= 2432) the laminar Schmidt number. The constants follow McPhee et al. (1987). The roughness height, z_0, is assumed to be constant and equal to 0.05 m according to Leppäranta and Omstedt (1990).

2.5. *Turbulence model*

The turbulence model used is a buoyancy-extended two-equation model of turbulence; one equation for the turbulent kinetic energy, k, and another for the dissipation rate of turbulent kinetic energy, ε. The generation of turbulence is calculated from current shear, associated with the wind or the ice drift, and buoyancy production, associated with cooling to the temperature of maximum density and salt rejection due to freezing ice.

The turbulence equations read:

$$\frac{\partial k}{\partial t}=\frac{\partial}{\partial z}\left(\frac{\nu_T}{\sigma_k}\frac{\partial k}{\partial z}\right)+P_s+P_b-\varepsilon, \tag{30}$$

$$\frac{\partial \varepsilon}{\partial t}=\frac{\partial}{\partial z}\left(\frac{\nu_T}{\sigma_\varepsilon}\frac{\partial \varepsilon}{\partial z}\right)+\frac{\varepsilon}{k}(C_{1\varepsilon}P_s+C_{3\varepsilon}P_b-C_{2\varepsilon}), \tag{31}$$

$$P_s=\nu_T\left[\left(\frac{\partial U}{\partial z}\right)^2+\left(\frac{\partial V}{\partial z}\right)^2\right], \tag{32}$$

$$P_b=\nu_T g\left[-\frac{2\alpha(T-T_M)}{\sigma_H}\frac{\partial T}{\partial z}+\frac{\beta}{\sigma_S}\frac{\partial S}{\partial z}\right], \tag{33}$$

$$\nu_T=C_\mu\frac{k^2}{\varepsilon}, \tag{34}$$

where P_s is the production due to shear, P_b is production/destruction due to buoyancy, σ_k and

Table 1. *Model constants. The constants in the heat flux formulations are given in connection with the equations*

Constant	Value	Unit
C = ice strength coefficient	20	—
C_p = specific heat of water	$4.2 \cdot 10^3$	J kg^{-1} K^{-1}
C_μ = constant in the turbulence model	0.09	—
C_{1_ε} = constant in the turbulence model	1.44	—
C_{2_ε} = constant in the turbulence model	1.92	—
C_{3_ε} = constant in the turbulence model	0.8	—
h_s = snow thickness	0.1	m
k = water stress coefficient	1.0	Ns m^{-3}
k_i = thermal conductivity of ice	2.0	W m^{-1} K^{-1}
k_s = thermal conductivity of snow	0.3	W m^{-1} K^{-1}
L_i = latent heat of ice	$3.34 \cdot 10^5$	J kg^{-1}
T_M = temperature for maximum density	3.2	°C
u_{free} = free ice drift	$0.03 U_a$	m s^{-1}
X_{dim} = ice cover dimension	$1.5 \cdot 10^5$	m
α_1 = constant in the equation of state	$5.6 \cdot 10^{-6}$	(°C)$^{-2}$
α_2 = constant in the equation of state	$8.1 \cdot 10^{-4}$	(‰)$^{-1}$
σ_k = Prandtl/Schmidt number	1.4	—
σ_ε = Prandtl/Schmidt number	1.3	—
μ_0 = ice strength coefficient	$4 \cdot 10^1$	N kg^{-1}
ρ_i = ice density	$9.2 \cdot 10^2$	kg m^{-3}
ρ_0 = reference density	$1 \cdot 10^3$	kg m^{-3}

σ_ε are Prandtl/Schmidt numbers, C_μ, C_{1_ε}, C_{2_ε} and C_{3_ε} are constants, see Table 1. The surface boundary conditions for turbulent kinetic energy, k, and its dissipation rate, ε, are related to the friction velocity and the net heat flux at the air/sea interface. At the lower boundary, a zero flux condition is used.

The model has been used by the present author and his colleagues in several geophysical applications, see, e.g., Svensson (1979) and Leppäranta and Omstedt (1990).

3. Details of calculations

To explore the mathematical formulation in Section 2, and particularly the formation, growth and decay of an ice cover, some sensitivity and verification studies were carried out. The results from these studies are presented in Sections 4 and 5 respectively.

In the ice drift calculation, eqs. (3) and (5), only deformation to the north was considered, and ice drift to the south was thus assumed to be equal to the free drift. As deformation also may occur at other coasts in the Bothnian Bay, the ice drift was calculated on the basis of the wind vector equal to the wind speed, but with the sign of the north/south wind component. During drift to the south, the ice cover was allowed to spread in the ice drift calculation, and the ice concentration was only changed due to thermal forcing.

As the ice front movements are considered in eq. (6), the boundary conditions for the ocean model were assumed to be equal to the temperature of freezing when the ice cover started to grow. Thus, open boundary conditions were used as long as no sea ice was present in the Bothnian Bay. When ice started to form (defined as when an ice concentration of 5% was observed), the boundary conditions were changed into the ice conditions. The heat flow from the ocean, eq. (16), was then calculated by the ocean model. The ice salinity in the boundary condition for the salinity equation (27) was assumed to be 50% of the surface water salinity. This is a reasonable rule of thumb for freezing sea ice but overestimates the ice salinity during melting. The

drainage of brine from the growing sea ice is thus neglected.

The ocean model, eqs. (17)–(34), in their finite difference form, were integrated forward in time using an implicit scheme and a standard tridiagonal matrix algorithm, Svensson (1986). The model constants are given in Table 1 and in connection with the heat flux equations, in Section 2.

4. Sensitivity studies

The formation, growth and decay of a sea ice cover can be calculated on the basis of the theory presented in Section 2. Even though several simplifications have been introduced, the model has quite a large number of constants and parameters which can vary considerably. A complete sensitivity study is not dealt with in the present paper. Instead only some basic aspects of the model will be illustrated below.

4.1. Ridging

Modelling ice dynamics in coastal seas, Overland and Pease (1988) argued that the ice strength (P) should depend on the square of the ice thickness, or:

$$P = \rho_i \mu_0 h_i^2 \exp(-C(1 - A_i)), \tag{35}$$

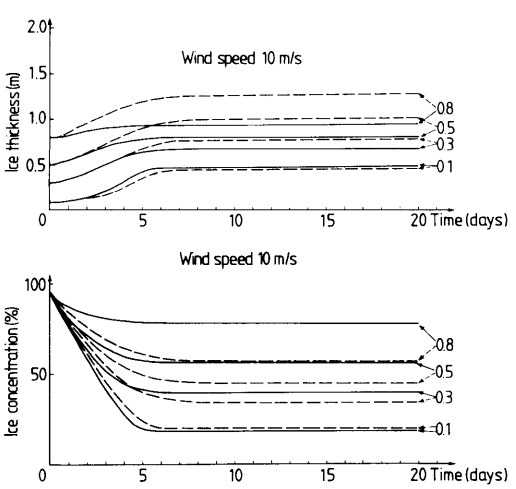

Fig. 3. A model comparison between the ice strength parameterization according to Overland and Pease (1988) (fully drawn lines) and Hibler (1979) (dashed lines). The numbers indicate the initial ice thicknesses.

where μ_0 is an ice strength parameter and C a constant. This formulation differs from the more traditional sea ice parameterization by Hibler (1979), where a linear relation is proposed:

$$P = P_* h_i \exp(-C(1 - A_i)), \tag{36}$$

where P_* is assumed to be a constant. From the two formulations one can see that ice strength is assumed to depend on the ice concentration in a similar manner.

To test the different parameterizations, some idealized calculations were performed. The sea area was initially assumed to be almost covered with ice of a constant thickness. For different wind speeds and initial ice thicknesses the two ice strength parameterizations were compared. In Fig. 3, results from one situation with an onshore wind of 10 m/s are illustrated.

The constants used are $P_* = 2 \cdot 10^4$ (Nm^{-2}), $C = 20$, and $\mu_0 = 4 \cdot 10^1$ (N kg^{-1}). These constants imply that the ice strength formulations are assumed to be equal at an ice thickness of about 0.5 m. The ice strength constant μ_0 is one order of magnitude larger than that used by Overland and Pease (1988). This is due to the fact that the horizontal scale considered in the present model is the whole basin, and on that scale ridging probably never doubles the ice thickness, see further discussion in Section 5.

In general, the parameterization by Hibler (1979) predicts more ridged ice, and in the case of higher wind speeds the values become quite high. From the verification studies in Section 5, the different ice strength parameterizations do not, however, indicate any basic differences in the results. Recent field data from the Bothnian Bay, Leppäranta (1987), indicate that the average ice strength during cold periods may reach values larger than $P_* = 2.2 \cdot 10^5$ Nm^{-2} (ice thickness equal to half a meter), which is one order of magnitude greater than what is generally used in ice models. We may thus conclude that the ice strength parameterization is still open for improvements.

4.2. Ice formation

The ice formation is due partly to vertical growth and partly to horizontal advance. In general, ice formation starts in the Bothnian Bay in November when the radiation from the sun is small. The corresponding model response to

typical early winter conditions is illustrated in Figs. 4 and 5. The basic assumption is that the sea temperature is equal to the freezing temperature. The sky is covered with clouds, and the relative humidity is 90%. The first test is given in Fig. 4, where the wind is assumed to be zero and the air temperature is varied. The horizontal advance illustrates that the basin will be almost ice-covered within one to two weeks, in the case of air temperatures of −25°C and −5°C respectively. If the cloudiness decreases, the freeze-up becomes, of course, much more rapid.

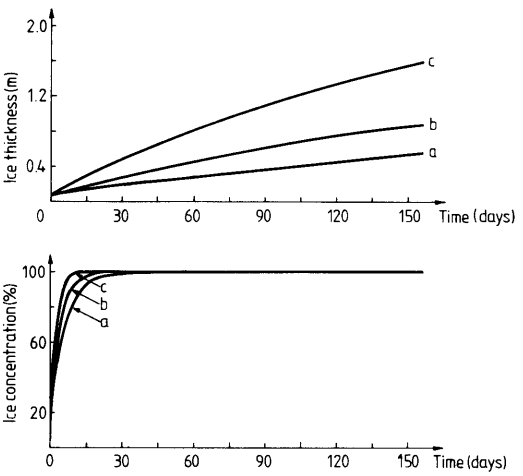

Fig. 4. Model simulation of ice formation during calm wind conditions but with variable air temperatures. The three cases are: (a) an air temperature of −5°C and a net heat loss of 66 W m^{-2}, (b) an air temperature of −10°C and a net heat loss of 95 W m^{-2}, and (c) an air temperature of −25°C and a net heat loss of 166 W m^{-2}.

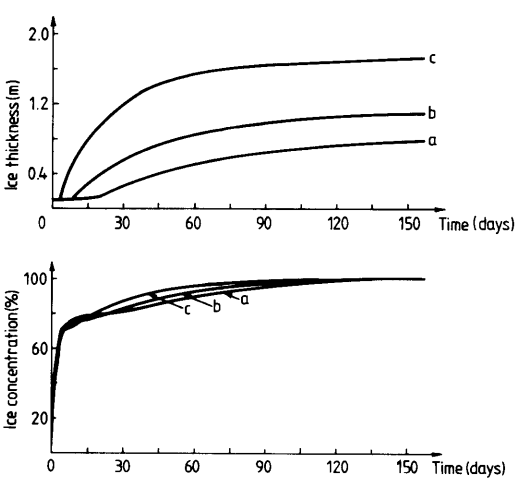

Fig. 5. Model simulation of ice formation during constant air temperature (−5°C) but with variable wind speeds. The three cases are: (a) a wind speed of 5 m s^{-1} and a net heat loss of 147 W m^{-2}, (b) a wind speed of 10 m s^{-1} and a net heat loss of 240 W m^{-2}, and (c) a wind speed of 25 m s^{-1} and a net heat loss of 517 W m^{-2}.

If wind effects are added to the model (Fig. 5), one has to keep in mind that besides ridging the net heat loss increases as both air temperature and wind enter into the heat flux equations. From the figure one can notice how the first ice formation phase rapidly increases the ice concentration. The ice thickness during this phase is almost constant. At a certain ice concentration the horizontal advance is decreased, and ridging dramatically increases the thickness. During the ridging phase the ice drift is highly influenced by the shore and decreases slowly to zero due to ice pressure. It should also be noted that even though the net heat flux is higher when the wind is blowing, the time to cover the basin is much larger due to ice deformation.

4.3. Ice decay

The ice decay includes break-up, vertical melting and horizontal retreat. Some response characteristics of the model are discussed below for the case of an almost ice-covered basin with a mean ice thickness of 0.5 m. The first situation considered is melting without winds (Fig. 6). From the figure one can notice the importance of sun radiation for the decay of the ice cover. If also wind is introduced (Fig. 7), the ice concentration decreases even faster due to ridging. Winds therefore strongly influence how fast the ice will decay in the model. The figures also illustrate that the main decrease is predicted to occur in the ice concentration and not in the ice thickness. This is also in agreement with what one can observe from ice charts during the spring warming period.

The importance of ice albedo during ice decay is not dealt with here. Instead the reader is referred to Maykut and Perovitch (1987). In Section 5, the model is tested during three winter periods using observed meteorological forcing. The main objective was to evaluate whether the

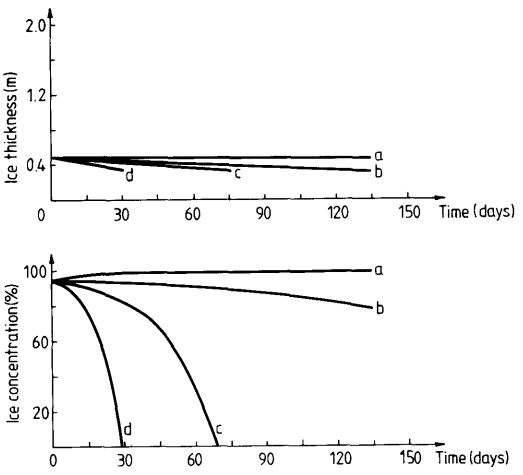

Fig. 6. Model simulations of break-up and melting ice during calm wind and with a constant air temperature (5°C), but with variable heat fluxes due to sun radiation. The four cases are: (a) no sun radiation and a net heat loss of 34 W m^{-2}, (b) a sun radiation of 50 W m^{-2} and a net heat gain of 16 W m^{-2}, (c) a sun radiation of 100 W m^{-2} and a net heat gain of 66 W m^{-2}, and (d) a sun radiation of 150 W m^{-2} and a net heat gain of 166 W m^{-2}.

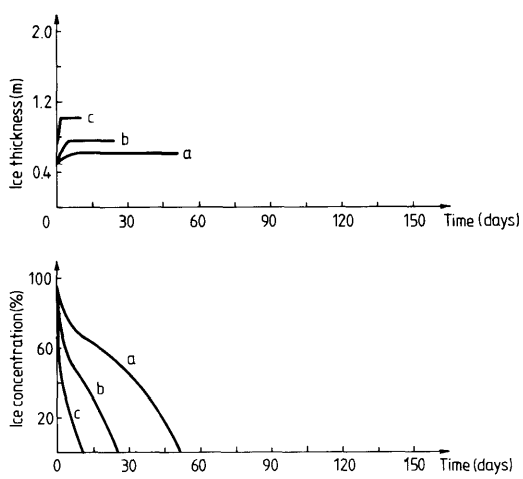

Fig. 7. Model simulations of break-up and melting ice during constant air temperature (5°C) but with variable on-shore wind speeds. The three cases are: (a) a wind speed of 5 m s^{-1} and a net heat gain of 56 W m^{-2}, (b) a wind speed of 10 m s^{-1} and a net heat gain of 103 W m^{-2}, and (c) a wind speed of 25 m s^{-1} and a net heat gain of 244 W m^{-2}.

model can be used for simulating the winter thermal regime of a semi-enclosed sea, such as the Bothnian Bay, or not.

5. Verification studies

The model given in Section 2 is here tested with data from the Bothnian Bay. The Bothnian Bay (Fig. 1) is the northern extension of the Baltic Sea with a maximum depth of 126 m and a mean depth of 41 m. The depth of the upper, well mixed layer varies between 30 and 50 m and has a salinity of 3.0–3.5‰, while the bottom layer salinity is in the range of 4.0–4.5‰. A typical residence time is 3 years. Ice formation starts in the northern archipelago in general in the beginning of November. The ice reaches its maximum extent in March and has in general melted away by the beginning of June. Periods with rapid horizontal ice cover advance due to calm and cold weather are often interrupted by periods of horizontal retreat due to windy weather conditions. Rafting and ridging are common features in the Bothnian Bay.

The ice cover in the Bothnian Bay may vary considerably. In Fig. 8 a vertical thin section of sea ice are shown. The classification scheme distinguished between Granular Ice and Columnar Ice, where Granular Ice could either be of snow or ice origin. The ice cores were sampled during BEPERS (Bothnian Bay Experiment in Preparation for ERS-1) in March, 1988. The figure illustrates that mechanical processes are important processes for ice mass calculations in the Bothnian Bay.

Statistical sea ice properties from the Bothnian Bay are illustrated in Fig. 9. All data are horizontally averaged for the whole Bothnian Bay and based upon data from a period of 16 years. From the figure one can notice a large scatter, and situations when the Bothnian Bay was almost ice-covered with level ice thicknesses varying from 0.2 to 0.8 m. Due to ridging, the ice mass increases. This can be represented by an equivalent thickness, which includes frequency of ridged ice and amount of ridges. In Fig. 10, the ratio between the equivalent and the level ice thickness are plotted against the ice level thickness. All data are horizontally averaged over the Bothnian Bay, and again one can notice a large

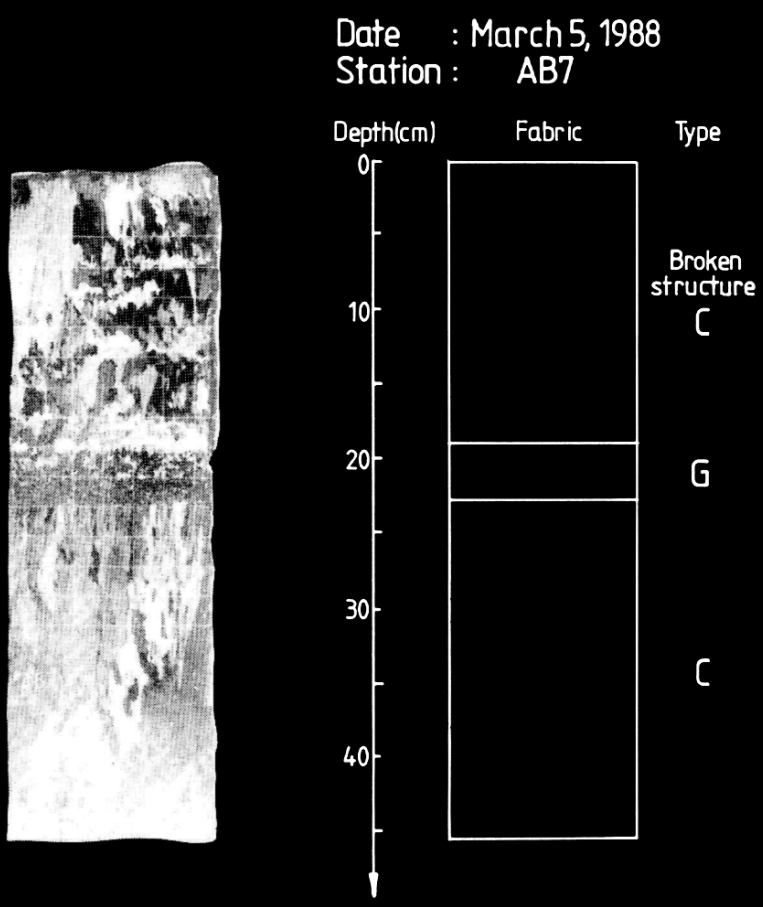

Fig. 8. A vertical thin section of sea ice taken from the BEPERS-88 experiment. The different ice types are: C = Columnar Ice, and G = Granular Ice.

scatter. Also, that the ice amount due to ridged ice adds less than about 60% to the level ice thickness.

In Subsections 5.1–5.3, data from three ice winters will also be considered. The data used are based upon ice charts from the season 1972/73, 1973/74 and 1974/75 together with weather data from one synoptic weather station, Holmögadd (63°36′N, 20°46′E). The weather data (wind, air temperature, total amount of cloudiness, and relative humidity) were used in the calculation of the heat and radiation fluxes and the wind stress. Of course, one weather station can only roughly represent the meteorological forcing over the whole basin. The meteorological forcing was calculated with a time resolution of 3 hours. This should be compared with the ice data which represent averaged data over at least 2 days. This implies that the verification study is mainly limited by the quality of ice data.

The ice data were based upon information taken from routinely analysed ice charts. Generally, these charts synthesize all available data and present them in a qualitative rather than quantitative form twice each week. The most important data are from the ice breakers, which report visual as well as radar observations. Also some information from helicopter reconnaisances, merchant ships, aviation and coastal stations add further knowledge.

Today, satellites add quite detailed information, particularly on ice concentration. In the

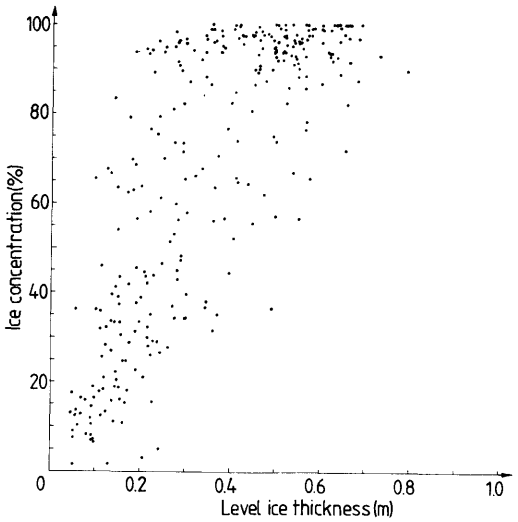

Fig. 9. The horizontal mean ice concentration and level thickness in the Bothnian Bay, based upon 16 years data.

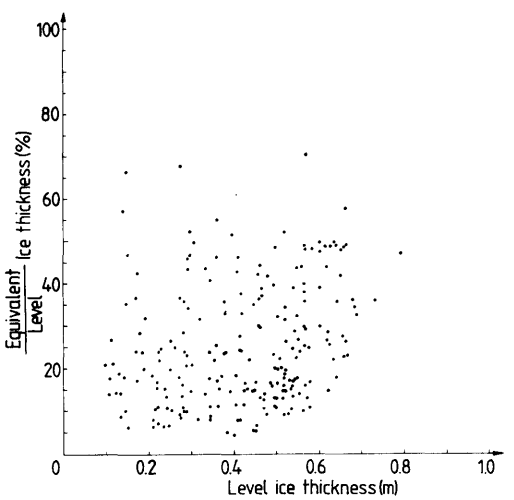

Fig. 10. The horizontal ratio of equivalent to level ice thickness and level ice thickness in the Bothnian Bay based upon 16 years data.

beginning of 1970 the satellite data were still under development and only used now and then. The most reliable ice data are probably those of ice extension (the total ice concentration). This is also the main parameter used in the present verification study.

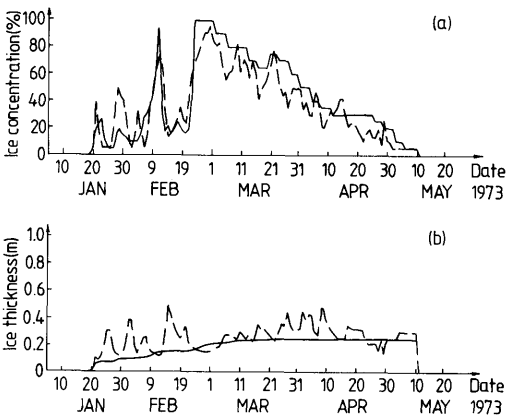

Fig. 11. Simulations of the ice winter 1972/73. (a) Ice concentration based on calculated (dashed line) and observed (fully drawn line) data. (b) Ice thicknesses based on the present model (dashed line) and on the cold degree-days method (fully drawn line).

5.1. The winter of 1972/73

The ice winter of 1972/73 was extremely mild. The first ice was reported from the northern archipelago in the beginning of November. The main ice formation did not, however, start until the beginning of February. Southerly winds forced the ice northwards, and on the 13 February the major parts of the Bothnian Bay were open again. At the end of February the maximum ice extension was reached. Thereafter the ice cover slowly decreased with periods of ice ridging.

In Fig. 11a, the calculated and observed ice concentrations are illustrated. Some rapid events of freezing occurred in January and February, but due to ridging the ice cover was decreased. From March the ice cover slowly decreased due to deformation and melting. The corresponding mean ice thicknesses are given in Fig. 11b. During ridging the ice thicknesses increase, while periods with rapid horizontal ice cover advance are associated with decreasing ice thicknesses. This rather strange behaviour is due to the fact that only the mean ice thickness is illustrated in the figure and that new ice influences this thickness quite a lot. The mean ice thickness is compared with a thickness calculated from the cold degree–days method, where the constant is put equal to 0.02. This method is more appropri-

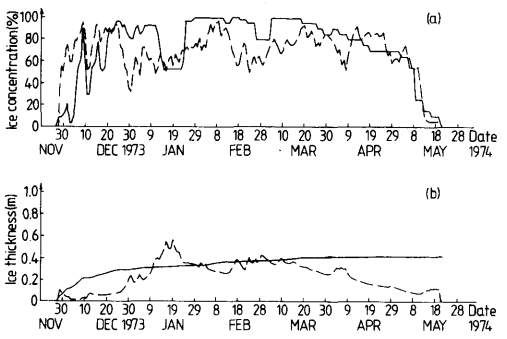

Fig. 12. Simulations of the ice winter 1973/74. (a) Ice concentration based on calculated (dashed line) and observed (fully drawn line) data. (b) Ice thicknesses based on the present model (dashed line) and on the cold degree-days method (fully drawn line).

ate for calculating the ice thickness in the landfast ice region, and the comparison thus indicates the importance of level ice growth to new ice formation, ridging and melting.

The results from the winter of 1972/73 show that the model simulates the sea ice evolution realistically during the whole winter. The observed ice concentrations show less variation than the calculated ones, probably due to the difficulties in making ice charts.

5.2. *The winter of 1973/74*

The ice winter of 1973/74 was mild, with ice formation starting at the end of November. In December new ice formed rapidly, but due to rather strong winds the Bothnian Bay was not ice-covered until late December. During March periods with new ice formation was interrupted with periods of ice ridgings. The ice field melted slowly, and almost all the ice had gone by the middle of May.

In Fig. 12a, the calculated and observed ice concentrations are illustrated. The initial growth started in late November, and the Bothnian Bay was almost ice-covered the whole winter. In the model calculation one can see how the initial ice cover advance is quite well modelled; however, the ice thickness (Fig. 12b) indicates that melting almost overcomes freezing in the initial phase. The reason is the fact that all ocean heat is introduced in the model as soon as the ice front starts to move. In reality, horizontal temperature gradients are always present in the Bothnian Bay due to different cooling in the coastal zone compared with the open basin area. In January, an important ridging event occurs. Finally, in April, the spring warming starts with a decrease in ice concentration due to melting and deformation.

The main deviation between calculations and observations is associated with the very thin ice calculated in the beginning of the ice season. The reason is probably due to horizontal temperature gradients in the sea, which are not dealt with in the model. The calculations are also more sensitive to the forcing than what was observed in the ice chart. The most probable explanation is that the thin ice thickness in the calculations underestimates the ice strength and therefore the resistance due to compression.

5.3. *The winter of 1974/75*

The ice winter of 1974/75 was extremely mild. The first ice was reported on the 13 November from the northernmost skerries, but the main ice formation started at the end of December. Strong winds between south and southwest pressed the ice against the northern coast in late January. The ice extension reached its maximum on the 17 February. Along the Finnish coast heavy ice pressure occurred. In April strong northerly winds drifted the ice southwards. At the end of April, when the temperature increased with westerly winds, the ice cover retreated rapidly.

In Fig. 13a, the calculated and observed ice concentrations are illustrated. Rapid freezing events are modelled and observed in the beginning of the ice season. In the calculations the ice concentrations seem, however, to be overestimated. This is probably due to the presence of horizontal gradients in the sea, which is not taken into account in the present theory. In late January a period with ridging is modelled (see Fig. 13b), and later the sea is frozen over again. In April the spring warming starts with a rapid decrease in ice concentration due to melting and ice deformation.

The main deviation between calculations and observations is associated with the melting period, where model calculations predict higher ice concentrations due to new ice formation compared with the ice chart data. During April 1975, a sea ice field experiment from the Finnish research vessel Aranda took place. During this

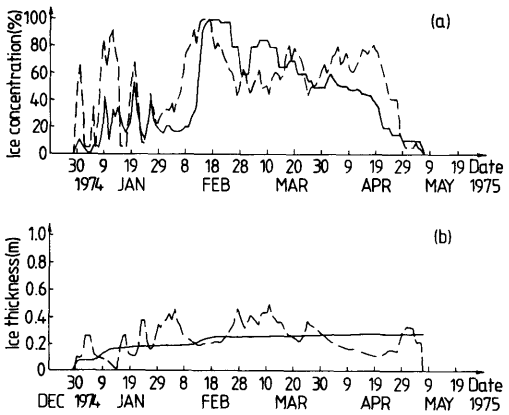

Fig. 13. Simulations of the ice winter 1974/75. (a) Ice concentration based on calculated (dashed lines) and observed (fully drawn line) data. (b) Ice thicknesses based on the present model (dashed line) and on the cold degree-days method (fully drawn line).

experiment new ice formation was observed (see Fig. 1 in Leppäranta and Omstedt, 1990). The observations indicate that new ice formation is underestimated in the ice chart data.

6. Discussion

The sensitivity and verification studies illustrate that the present mathematical approach can reproduce several features, which are of importance for the winter ice regime in semi-enclosed seas. The rapid freezing-over in the initial ice phase seems to be correctly modelled as well as ridging and horizontal retreat. The results thus give confidence that the main physical processes are reasonably understood. The calculations can, however, only be regarded as a rough estimation of the importance of the different processes. The approach is probably sound, but several aspects are oversimplified. For example, ridging occurs in the Bothnian Bay in all directions and with a range of different ice thicknesses and ice types. Winds from the south cause heavy ridging, but this is also true for winds from the north-east, which are not dealt with in the present paper. The assumption of a horizontal homogeneous ocean can also be of doubtful value for the Bothnian Bay, at least during initial ice formation, when the coastal areas often reach freezing temperatures while the open basin is generally at least one degree Celsius above the freezing point. Horizontal temperature gradients are also formed during spring warming. These aspects obviously imply that more dimensions should be considered in the construction of ice–ocean models. However, with the many complicated factors associated with ice–ocean interaction in mind, the model simulations can be regarded as being quite satisfactory.

7. Summary and conclusions

The main objective of the present study was to examine whether a one-dimensional model approach could be developed for the winter thermal regime in a semi-enclosed sea such as the Bothnian Bay, or not. The mathematical model presented in the paper therefore introduced a sea ice model on top of a one-dimensional ocean model. The basic assumption in the sea ice model was that ridging only occurs during on-shore winds. During off-shore winds no ice strength was assumed, and accordingly the ice drifted freely with a constant wind factor.

The thermodynamic calculations considered the heat balance between open water and air and the heat exchange between water and ice. The upper boundary conditions for the ocean model were changed from open water conditions to ice conditions when a sea ice concentration of 5% was observed. The sea ice equations focused attention on the question of whether the ice edge advances or retreats. Only horizontal mean properties were considered, and the model was examined on the basis of sensitivity and verification studies with the Bothnian Bay in mind.

The conclusions from the paper may be summarized as:

- A one-dimensional modelling approach for sea-ice in a semi-enclosed sea as the Bothnian Bay can be used, giving quite realistic information about ice formation, growth and decay.
- Horizontal gradients in the sea and in the ice imply that there is a general need for a two- or three-dimensional model, particularly for the initial advance of the ice edge and for the ice deformation calculations.

8. Acknowledgements

This work has been financed by the Swedish Natural Science Research Council and the Swedish Administration of Shipping and Navigation. Special thanks are given to Jörgen Sahlberg and Jan-Erik Lundquist for supporting me with ice data, to Matti Leppäranta for valuable discussions about plastic ice drift, to Peter Lemke for valuable comments on an earlier draft of this paper, and to an anonymous reviewer for several improvements. Also the drawing and the printing by Ann-Margreth Holst and Vera Kuylenstierna are gratefully acknowledged.

REFERENCES

Bauer, J. and Martin, S. 1983. A model of grease ice growth in small leads. *J. Geophys. Res. 88*, 2917–2925.

Bodin, S. 1979. A predictive numerical model of the atmospheric boundary layer based on the turbulent energy equation. *Report Meteorology and Climatology No. 13*, SMHI, S-601 76, Norrköping, Sweden, 139 pp.

Fichefet, Th. and Gasper, Ph. 1988. A model study of upper ocean–sea ice interactions. *J. Phys. Oceanogr. 18*, 181–195.

Friehe, C. A. and Schmitt, K. F. 1976. Parameterization of air–sea interface fluxes of sensible heat and moisture by the bulk aerodynamic formulae. *J. Phys. Oceanogr. 6*, 801–809.

Hibler III, W. D. 1986. Ice dynamics. In: *The geophysics of sea ice* (ed. N. Untersteiner). The NATO ASI Series, B 146. New York: Plenum, 577–640.

Hibler III, W. D. 1979. A dynamic thermodynamic sea ice model. *J. Phys. Oceanogr. 9*, 815–846.

Langleben, M. P. 1972. The decay of an annual cover of sea ice. *J. Glaciology 11*, No. 63, 337–344.

Lemke, P. 1987. A coupled one-dimensional sea ice–ocean model. *J. Geophys. Res. 92*, 13164–13172.

Leppäranta, M. 1983. A growth model for black ice, snow ice and snow thickness in subarctic basins. *Nordic Hydrology*, 59–70.

Leppäranta, M. 1987. Field Experiment SEA ICE-85 in midwinter in the Bay of Bothnia: Ice observations. *MERI, No. 15*. Finnish Inst. of Marine Research. Finland, 15–33.

Leppäranta, M. and Hibler III, W. D. 1985. The role of plastic ice interaction in the Marginal Ice Zone dynamics. *J. Geophys. Res. 90*, 11899–11909.

Leppäranta, M. and Omstedt, A. 1990. Dynamic coupling of sea ice and water for an ice field with free boundaries. *Tellus 42A*, 482–495.

Maykut, G. A. 1986. The surface heat and mass balance. In: *The geophysics of sea ice* (ed. N. Untersteiner). The NATO ASI Series, B146. Plenum: USA, 395–463.

Maykut, G. A. and Perovitch, D. K. 1987. The role of short wave radiation in the summer decay of a sea ice cover. *J. Geophys. Res. 92*, 7032–7044.

McPhee, M. G. 1986. The upper ocean. In: *The geophysics of sea ice* (ed. N. Untersteiner). The NATO ASI Series, B 146. Plenum: USA, 339–394.

McPhee, M. G., Maykut, G. A. and Morrison, J. H. 1987. Dynamics and thermodynamics of the ice/upper ocean system in the marginal ice zone of the Greenland Sea. *J. Geophys. Res. 92*, 7017–7031.

Mellor, G. L., McPhee, M. G. and Steele, M. 1986. Ice–sea water turbulent boundary layer interaction with melting and freezing. *J. Phys. Oceanogr. 16*, 1829–1846.

Omstedt, A. 1985. Modelling frazil ice and grease ice formation in the upper layers of the ocean. *Cold Regions Science and Tech. 11*, 87–98.

Omstedt, A. 1990. Modelling the Baltic Sea as thirteen sub-basins with vertical resolution. *Tellus 42A*, 286–301.

Omstedt, A., Sahlberg, J. and Svensson, U. 1983. Measured and numerical simulated autumn cooling in the Bay of Bothnia. *Tellus 35A*, 231–240.

Overland J. E. and Pease, C. H. 1988. Modeling ice dynamics of coastal seas. *J. Geophys. Res. 93*, 15619–15637.

Pease, C. H. 1987. The size of wind-driven coastal polynyas. *J. Geophys. Res. 92*, 7049–7059.

Røed, L. P. 1984. A thermodynamic coupled ice–ocean model of the marginal ice zone. *J. Phys. Oceanogr. 14*, 1921–1929.

Sahlberg, J. 1988. Modelling the thermal regime of a lake during winter season. *Cold Regions Science and Technology 15*, 151–159.

Stössel, A. 1985. Thermodynamic calculations of ice production in the northern Baltic Proper. *Dt. Hydrogr. Z. 38, H. 6*, 261–284.

Svensson, U. 1979. The structure of the turbulent Ekman layer. *Tellus 31*, 340–350.

Svensson, U. 1986. PROBE—An instruction manual. *Report Oceanography No. 10*, SMHI, S-601 76 Norrköping, Sweden, 90 pp.

Svensson, U. and Omstedt, A. 1990. A mathematical model of the ocean boundary layer under drifting melting ice. *J. Phys. Oceanogr. 20*, 161–171.

Yaglom, A. M. and Kader, B. A. 1974. Heat and mass transfer between a rough wall and turbulent fluid flow at high Reynolds and Peclet numbers. *J. Fluid Mech. 62*, 601–623.